Proceedings of ICFD 10:
Tenth International Congress of Fluid Dynamics
December 16-19, 2010, Stella Di Mare Sea Club Hotel, Ain Soukhna, Red Sea, Egypt

ICFD10-EG-3004

AN INVESTIGATION OF THE EFFECT OF ANTI-VORTEX FILM COOLING ON A FLAT PLATE

Mostafa Abdel-Mohimen Hussein
Shoubra Faculty Of Engineering, Benha University

Tarek A. Mekhail
South Valley University

Samir S. Ayad
Shoubra Faculty Of Engineering, Benha University

Karam M. El-Shazly
Shoubra Faculty Of Engineering, Benha University

ABSTRACT

An experimental test rig is constructed to study different configurations of the film cooling technique developed at NASA Glenn Research Center. This technique depends on adding a pair of cylindrical anti-vortex holes branching out from the main cylindrical film cooling holes to mitigate the effect of kidney vortices that causes the jet to lift off. Four different values of velocity ratios (VR), (Coolant Jet Velocity/Main Stream Velocity) namely VR=0.5, 1.0, 1.5, and 2.0, are studied with three different positions of anti-vortex holes. A single row of 30o angled holes on a flat surface, which gives a zero pressure gradient along the downstream test surface, is taken as a baseline. The different holes configurations are tested. The numerical study is carried out using FLUENT commercial code using the k-ε model. The density ratio is taken in consideration. Numerical results are first compared with experimental values of temperatures and film cooling effectiveness and the comparisons verified the numerical model. Both of experimental and numerical studies show that the new technique improves the film cooling effectiveness. The numerical velocity vectors in the boundary layer region showed that the anti-vortex holes create reverse vortices against the main vortices that are created by the main hole. These reverse vortices help in keeping the coolant jet flow near the surface.

KEYWORDS:

Film Cooling, Anti-Vortex, Turbine Blade Cooling

INTRODUCTION

Film Cooling is the introduction of a secondary fluid (coolant or injected fluid) at one or more discrete locations along a surface exposed to a high temperature environment to protect that surface not only in the immediate region of injection but also in the downstream region [8]. Film cooling protects the surface directly by forming a protective layer of cold air as compared to internal cooling, where blade is cooled by extracting heat by convection. Film Cooling also provides cooling from internal convection in the film holes. Flat surface film cooling has been known and subjected to research for a long time. Goldstein et al. [9] described the effectiveness characteristics with lateral injection. The effectiveness following single hole of the inclination angle of 15 and 35 deg are investigated. They reported that the effect of lateral injection is to widen the temperature field and decrease the peak effectiveness for the blowing ratio of BR=0.5. For the higher blowing ratios, however, the lateral injection increases both the width of the temperature field and the peak film cooling effectiveness. Ammari et al. [1] also presented the effect of density ratio on heat transfer coefficient contours downstream of a film hole inclined 35° along the stream-wise direction for two different coolant-to-mainstream density ratios of 1.0 and 1.52 for a coolant blowing ratio of BR=1.46. Differences of 10% in film cooling occurred when coolant densities were changed. Bons et al.[3] studied the effect of high stream turbulence on film cooling effectiveness. At high free stream turbulence, heat transfer coefficients with film cooling are not as significantly as the film effectiveness. Film injection by itself produces high heat transfer coefficient enhancement due to high turbulent mixing between jet mainstream.

Andreopoulous and Rodi [2] studied the behavior of a single jet and mainstream interaction. There is a mutual deflection of the jet and the mainstream. The jet is pushed towards the bottom wall and the mainstream is deflected as if

the jet forms a solid boundary. At a low momentum ratio MR= 0.25, the mainstream pushes the jet to adhere to the bottom wall .At a higher momentum ratio MR=4.0, the jet penetrates into the mainstream before it is bent. There is a complicated three-dimensional separation region downstream of the jet in both cases, which is more pronounced at the higher momentum ratio. There have been vast studies in the field of interaction between coolant jet from inclined cylindrical holes and the mainstream flow. The interaction results in the formation of kidney vortices, i.e. a pair of counter rotating vortices as described by Haven et al. [10]. These vortices are detrimental to film cooling because it brings about two undesirable effects. Firstly, the hot mainstream air is forced to enter beneath the jet, thus heating the turbine blade wall. Secondly, the mutual interaction between the vortex pair tends to lift the jet off the turbine blade surface which diminishes the film cooling. Lemmon et al. [16] who showed that this vorticity is caused by the bending of the jet by the free-stream and not by viscous wall effects in the hole or plenum. For cases with varying density ratio, the momentum ratio is considered to be an even better predictor of jet lift-off than blowing ratio since higher density ratio jets will tend to remain attached to the surface at higher blowing ratios. Numerical prediction of flat surface film cooling also has been studied.

Alok Dhungel [5] investigated the enhanced cooling performance caused by addition of anti-vortex holes to the main cylindrical film cooling holes. Both heat transfer coefficient and film cooling effectiveness are determined experimentally downstream of the exit of the film cooling holes on a flat plate by a single test using the transient Infra Red thermography technique. A total of six different cases with variations in geometry and orientation of the anti vortex holes in relation to the main film cooling holes are thoroughly investigated. Results suggested that the presence of anti vortex holes mitigates the effect of the pair of anti vortices. Heidmann [11] and Heidmann et al [12] used a 3–D Navier-Stokes solver Glenn-HT which has been conceived and developed at NASA Glenn Research Center to study the "anti-vortex" film-cooling concept which is designed to mitigate the effects of the counter-rotating vortex pair, which reduces the effectiveness of circular cross-section film-cooling holes at moderate to high blowing ratios. Preliminary and improved designs concepts are developed in this study, although many parameters can be modified in an optimized design. The concept is applied in this study as a modification to a standard single row round film-cooling hole arrangement with the holes angled at 30 deg to the surface and a span-wise pitch of three hole diameters and is compared to the base line data of Dhungel et al [6].

The present work studies numerically and experimentally how to mitigate the effects of counter-rotating vortex pair by supplemented the main hole of the film cooling by two anti-vortex holes branched out from the main hole at different velocity ratios. A total of four different cases are studied. The film cooling holes are provided with a pair of anti-vortex holes in three cases. Each case has a different anti vortex hole geometry and orientation. Each test plate has a total of five film cooling holes with a span wise spacing of three primary hole diameters. Data are collected from the middle hole to reduce the effect of the side walls. The results of these cases are compared to a baseline case.

EXPERIMENTAL APPARATUS AND PROCEDURE

A schematic of the wind tunnel and the injectant supply system is shown in Figure (1). The wind tunnel is an open-circuit and subsonic one, with 4 to 1 contraction ratio nozzle. The nozzle leads to the test section which is a square duct (0.2m x 0.2m) with 2m length. A boundary layer trip wire of 2 mm diameter is located on the test plate just downstream of the nozzle exit [13]. Experiments are conducted at the fixed free-stream mean velocity of 8.6 m/s.

The film cooling jets supply unit consists of the air blower and the air control unit. The air blower forces air, to the test section through the air control unit. The air control unit consists of bypass and control valves to control the flow rate of air through the test section.

Experiments are conducted at the fixed free-stream mean velocity of 8.6 m/s. The injection hole diameter (D) is 10 mm and its length is 4 D inclined. The Reynolds number (Re_X) based on the distance between the trip wire and the hole center is 452,744. The velocity ratio (VR) is the ratio of the injectant mean velocity to free-stream mean velocity. The velocity ratio values are 0.5, 1.0, 1.5, and 2.0. The corresponding injectant Reynolds numbers (Re_D) are 2929, 5347, 7562, and 10695, respectively. The injectant is heated to a temperature twice the free stream temperature. The density ratio of injectant to free-stream due to the heating is 0.94. Thus, the momentum ratio values are 0.313, 1.044, 2.09 and 4.18 for velocity ratios of 0.5, 1.0, 1.5, and 2.0, respectively.

A row of five holes is located 80 D downstream of the trip wire. The hole spacing between the hole centers is 3 D. The bottom plate of the duct consists of an upstream plate, a film-hole plate, and a test plate. The test plate starts at x/D = 1.5. To prevent the adiabatic wall temperature elevation near the downstream edge of the holes, the injection holes are machined in the injection plate, not in the measurement plate.

To measure the temperature distribution on the test surface, the test surface has 13 rows of 7 holes drilled for 91 calibrated K-type thermocouples. The hole diameters are 1 mm and the distance from one to another is 5 mm. Thermocouples are inserted from the bottom of the Plexiglas so that the welded bead of the thermocouple is flush with the top surface. The thermocouples are glued into place with a two part Epoxy adhesive. The test surface and thermocouple beads are then covered with a thin foil to ensure a smooth continuous test surface. The thermocouples are centered at the front of the air jets of the middle hole as shown in figure (2).

Figure (3) shows the Baseline case, which is a flat plate with five inclined holes. The diameter of each hole is 10 mm

and the spacing between the holes is 3D. The length of holes is 4D. The holes are inclined to the horizontal at an angle of 30^o along the flow direction. A pair of anti-vortex holes are added each to all the five film cooling holes. The orientations and other geometries of the primary film cooling hole is the same as the baseline, only the features of the anti vortex film cooling holes are altered.

Three different geometries are investigated. The details of the geometry are presented in figure (4) and in table 1 where the distance between the center of the anti vortex holes and the center of the primary film cooling holes measured in the x-direction is represented by parameter 'a'. The similar distance measured in the y- direction is given by parameter 'b'. The angle measured in degrees between the axis of the primary film cooling holes and the anti vortex holes measured in the horizontal plane is represented by parameter 'P'. Similar angles measured in the front vertical plane and the side vertical planes are represented by parameters 'R' and parameter 'Q' respectively. Parameter 'D' and'd' represents the diameters of the primary film cooling holes and the anti vortex holes respectively.

Case-1: as shown in figure (5) (a), the anti vortex holes shoot out vertically upwards from the primary film cooling holes and thus the exit of the anti vortex holes is far upstream as compared to the exit of the primary film cooling hole. The anti vortex hole originate from the lower end of the primary film cooling hole

Case-2: as shown in figure (5) (b), the exit of the anti vortex film cooling holes are still upstream to the outlet of the primary film cooling hole but isn't far as compared to case-1. Both the anti vortex film cooling holes are symmetrical in orientation and location to the primary film cooling hole.

Case-3: as shown in figure (5) (c), the exit of the anti vortex film cooling hole geometry is in line with the primary film cooling holes. The anti vortex holes branch out near the middle point of the primary film cooling holes.

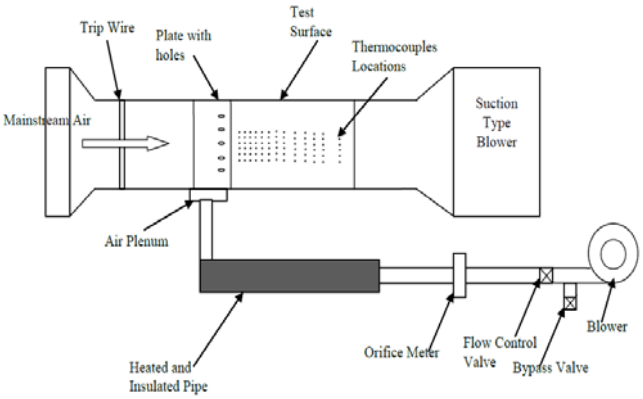

Fig. 1 Experimental Test Rig

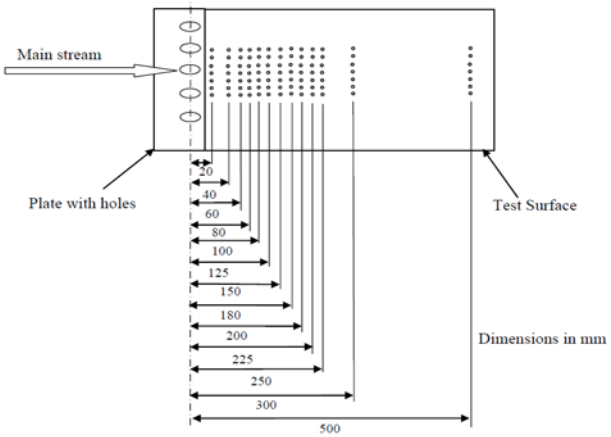

Fig. 2 Thermocouple Distribution on the Test Surface

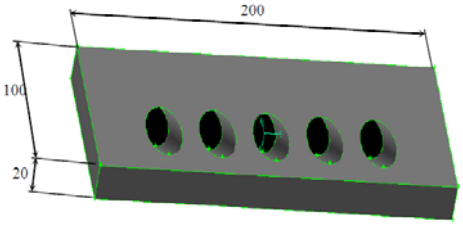

Fig. 3 Baseline Case

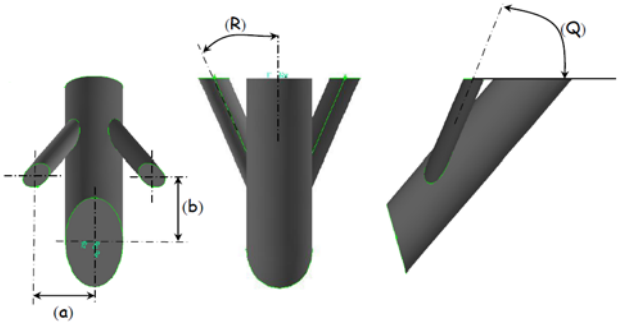

Top View Front View Side View

Fig. 4 the Anti-Vortex Hole Configuration

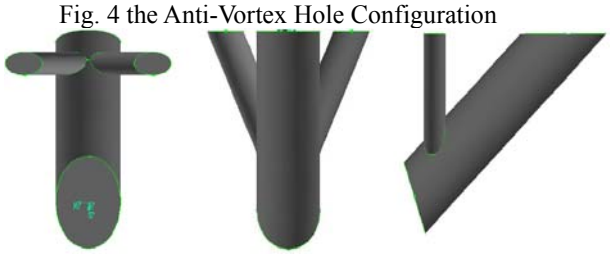

a) Case-1

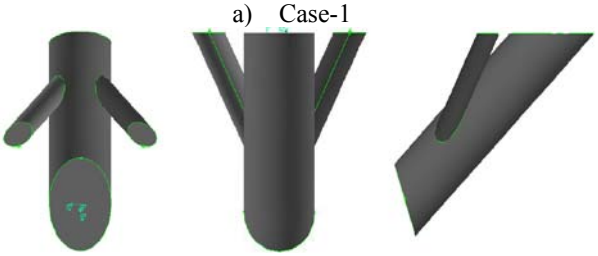

b) Case-2

c) Case-3

Fig. 5 Anti Vortex Hole Orientation

Table 1: Test Plate details (depending on fig. 4)

	Case 1	Case 2	Case 3
D (mm)	10	10	10
d (mm)	5	5	5
a (mm)	10	10	10
b (mm)	30	15	0
Q (^{o})	90	49.1	30
R (^{o})	30	30	30

NUMERICAL TECHNIQUE

Supporting the three-dimensional steady flow CFD studies are performed to gain a deeper insight into the flow field that is responsible for the observed coolant jet interaction with the mainstream. FLUENT is used to simulate film cooling for all anti-vortex geometries and compared to baseline case cylindrical holes.

The governing equations to be solved are the incompressible continuity, momentum, and energy equations and the transport equations for the turbulent kinetic energy, and dissipation added through the turbulence models. The fluid properties are assumed constant, which is a reasonable assumption compared to the corresponding experiments.

$$\frac{\partial U_i}{\partial x_i} = 0$$

$$\frac{\partial U_i}{\partial t} + \frac{\partial (U_j U_i)}{\partial x_j} = -\frac{1}{\rho}\frac{\partial P}{\partial x_i} + \frac{\partial}{\partial x_j}(2\nu S_{ij} - \overline{u_i' u_j'})$$

$$\frac{\partial T}{\partial t} + \frac{\partial (U_j T)}{\partial x_j} = \frac{\partial}{\partial x_j}(\frac{\nu}{Pr}\frac{\partial T}{\partial x_j} - C_p \overline{T' u_j'})$$

Where $\tau_{ij} = -\overline{u_i' u_j'}$ is known as the specific Reynolds stress tensor $C_p \overline{T' u_j'}$ and represents the specific turbulent heat flux. Both of these two terms need to be modeled. The computational grid is shown in Figure (6). The Figure highlights the grid quality near the hole intersection region for case (1). Symmetry boundary conditions are applied on all cases. This is done since the present study performed with a steady CFD analysis in which no flow can cross these planes because of symmetry. The boundary conditions are slightly different from the experiment and are prescribed at all three boundary surfaces of the computation domain. Mainstream conditions are maintained the same in all cases and the coolant flow rate is altered to change the velocity ratios. At solid walls, adiabatic boundary conditions are used, and no-slip boundary condition is set as:

$$U_w = 0, V_w = 0, W_w = 0, \overline{u_i' u_j'} = 0$$

where index w denotes the wall.

For the mainstream and the coolant jet velocity inlet, uniform profile is set. In our study, all the computations are performed with uniform flow inlet for the mainstream and the coolant jet. Standard total temperature value and inlet velocity are used at the mainstream inlet with flow normal to the inlet plane. The mainstream inlet is 20 D upstream of the main hole center line. The plenum inlet mass flow rate is adjusted to produce the blowing ratio desired. The plenum inlet total temperature is set to 2 times the mainstream inlet total temperature. The effect of density difference is taken in consideration and the density ratio is about of 0.94. A turbulence intensity of 1 percent and a turbulence length scale of 1D are specified at both the mainstream inlet and plenum inlet.

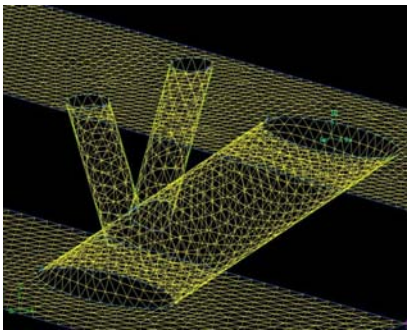

Fig. 6 Hole Intersection Grid Close-Up

The realizable k-ε model, in FLUENT, is used to solve the governing equations. An immediate benefit of the realizable k-ε model is that it more accurately predicts the spreading rate of both planar and round jets. It is also likely to provide superior performance for flows involving rotation, boundary layers under strong adverse pressure gradients, separation, and recirculation.

FLUENT is based on an unstructured grid solver using a finite volume approach for the solution of the Reynolds Averaged Navier-Stokes (RANS) equations. An unstructured computational grid is developed using the Gambit grid generator with approximately 1.8 million computational cells for each case. All the cases presented here converged to residual levels of the order of 10−8 for velocity components and energy equation and 10−5 for mass flow rate. An investigation of grid independence is carried out to find the proper mesh. The test is performed on the baseline.

The effectiveness measurements are made with the mainstream at ambient temperature, the coolant air heated, and the test surface unheated. Because the test surface is unheated and well insulated, it is assumed to be adiabatic. Therefore the local wall temperature at steady state conditions measured by the thermocouples is now the adiabatic wall temperature, Taw. Since the test surface is adiabatic, there is no heat transfer at the surface. As a result, the local film temperature, T_f, is equal to the corresponding adiabatic wall temperature, Taw. Now the

following equation can be used to calculate the film cooling effectiveness.

$$\eta = \frac{T_{aw} - T_m}{T_c - T_m}$$

This method of calculating the film effectiveness has been used by several researches such as Ou et al. [19] and Mehendale and Han [18]. A more precise method of estimating uncertainty in experimental results has been presented by Kline and McClintock [14]. The calculated uncertainty of the film cooling effectiveness is found to be about $\pm 1.55\%$.

RESULTS AND DISCUSSIONS

The detailed film cooling effectiveness is presented numerically because it is very difficult to present it experimentally as thermocouples are used to measure the test surface temperature.

QUANTITATIVE ANALYSIS:

Figure (7) shows the effect of velocity ratio on detailed film cooling effectiveness distributions for all four cases. For the baseline case, It is clear that the highest film cooling effectiveness occurring with the lowest velocity ratio (VR = 0.5). As the velocity ratio increases, there is a jet lift-off causing lower effectiveness.

For case 1, the effectiveness is higher than baseline case for all velocity ratios but the trend is different, as the velocity ratio increases the film effectiveness increases and covers bigger area. The anti-vortex pair cause reduced flow through the main hole and also supplements the overall coverage in the region between the holes. It appears that the anti vortex holes produce a small vortex pair counter to the main vortex pair. It is visible that the highest effectiveness occurs at velocity ratio of 2.0. The effect of this anti-vortex pair appears to mainly reduce the coolant momentum flux from the main holes.

For case 2, the anti vortex holes are still exit upstream of the main hole but more close to the main hole than in case 1. Like in case 1, the film effectiveness increases as the velocity ratio increases. But as shown in Figure (7) (c), the film effectiveness downstream the anti vortex holes decreases as the velocity ratio increases. So the regions between holes have less effectiveness than that in case 1.

In case 3, the highest film effectiveness is given by VR = 0.5 just downstream the film cooling holes. But as moving away from the film cooling holes, as the velocity ratio increases the film cooling fluid flow covers larger area than that is covered by the low velocity ratios. Figure (7) (d) shows that the film effectiveness covered area gets narrower as the flow moves downstream the film holes. It appears that the flow from anti-vortex holes moves side-by-side with the flow from the main holes.

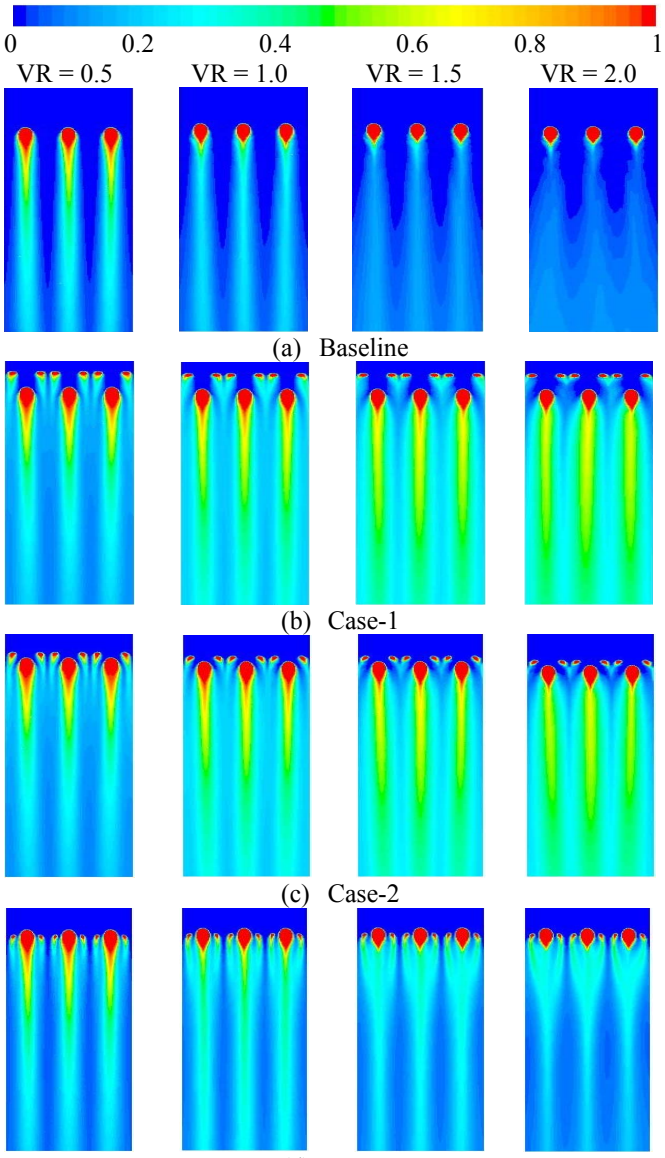

Fig. 7 Detailed Film Cooling Effectiveness Distributions for Studied Cases at different Velocity ratio

QUANTITATIVE ANALYSIS:

The span averaged is calculated for points from z/D = 1.5 to z/D = -1.5, it means that the span averaged film cooling effectiveness will be presented downstream the middle hole.

For VR = 0.5, Figure (8) shows that, for all cases the spanwise film effectiveness decreases as x/D increases. Case 1, case 2, and case 3 give high film effectiveness along the studied spanwise as compared with the baseline case. Generally all cases have the same trend and close to each other because at VR = 0.5, the momentum flux of the coolant jet is lower than that of the mainstream.

For VR = 1.0, Figure (9) shows that, baseline case has a different trend as compared to other cases. For baseline case, the film effectiveness starts from high value near the hole exit

and begins to decrease rapidly until x/D = 7 then the film effectiveness begins to increase slowly. Case 1 and case 2 have the same trend (as the coolant fluid is moving downstream the film holes, the film effectiveness decreases gradually). For case 3, as the coolant fluid is moving downstream the film holes, the film effectiveness decreases rabidly.

For VR = 1.5, Figure (10) shows that, the baseline film effectiveness has the same trend as the baseline film effectiveness for VR = 1.0 but with lower values. The numerical results show that, case 1 and 2 give the same spanwise film effectiveness with small decreasing as moving away from the film holes. But experimental results, case 1 and case 2 appear to have constant values of film cooling effectiveness along the test surface but with different values of each case. For case 3, the film effectiveness appears to start from a high value and decreases rapidly as the coolant jet fluid is moving downstream the film holes.

For VR = 2.0, Figure (11) shows that all cases still give the same trend as compared to that given by VR = 1.5. The highest spanwise averaged film cooling effectiveness is given by case 1. For both case 1 and case 2, the film effectiveness may be assumed to be constant along the studied area. Case 3 shows rabid decrease in film effectiveness as moving away from the film holes.

It can be seen that computational predictions for the studied cases are much higher than for the experimental data. It has always been indicated by previous film cooling prediction studies that the CFD results cannot predict the spreading of jets accurately and over predict centerline effectiveness. The spanwise averaged results show similarities as the cross-stream direction is averaged and washes out the local discrepancies between the predictions and experiments [20]. The maximum deviation between the numerical and experimental results as a ratio of numerical results for the overall area averaged film cooling effectiveness is about 2.3% at VR = 2.0 and 21.7% at VR = 0.5 for baseline case. But for case 1, the maximum deviation is about 34.9% at VR = 2.0 and 21.6% at VR = 0.5.

Figure (12) shows the overall area averaged film cooling effectiveness for all studied cases at different values of velocity ratios. The overall area averaged film cooling effectiveness is calculated for the area downstream the middle hole only. The overall area at which the averaged film cooling is calculated is ranged from x/D =0 to x/D = 25, and z/D = -1.5 to z/D = 1.5 for y/D =0. The figure shows that:

For baseline case, as the velocity ratio increases, the overall film effectiveness decreases. For case 1, as the velocity ratio increases, the overall film effectiveness increases. Case 1 gives the highest overall effectiveness at VR = 2.0. But for lower velocity ratios, all anti-vortex cases film effectiveness is closed to each.

Case 3 gives the lowest overall film effectiveness with higher velocity ratios if it is compared with case 1 and case 2. The overall area averaged film cooling effectiveness for case 3 may be assumed constant as the velocity ratio increases.

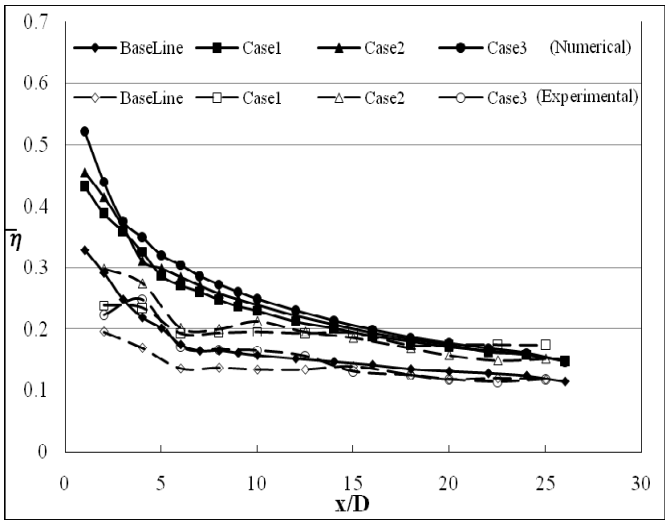

Figure (8) Effect of Anti Vortex Hole Geometry on Spanwise Averaged Film Cooling Effectiveness Distributions at VR = 0.5

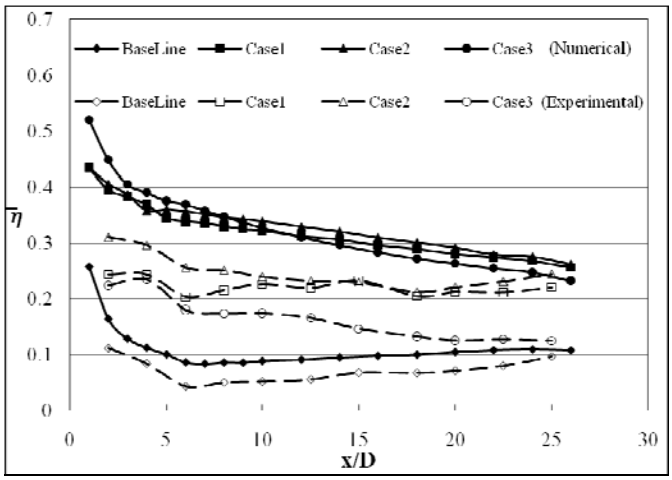

Figure (9) Effect of Anti Vortex Hole Geometry on Spanwise Averaged Film Cooling Effectiveness Distributions at VR = 1.0

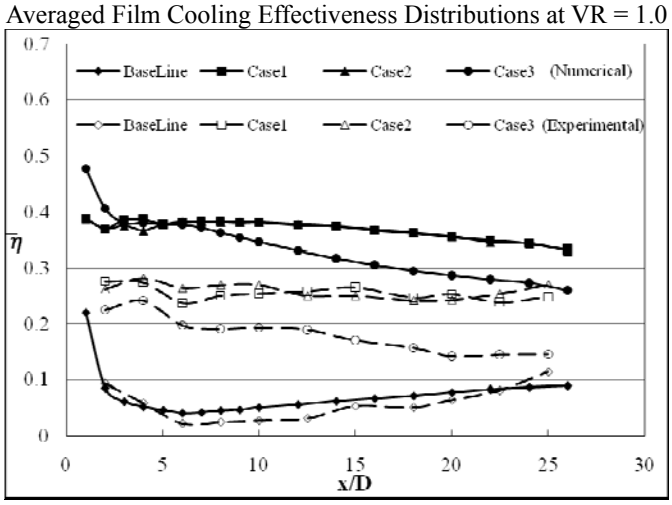

Figure (10) Effect of Anti Vortex Hole Geometry on Spanwise Averaged Film Cooling Effectiveness Distributions at VR = 1.5

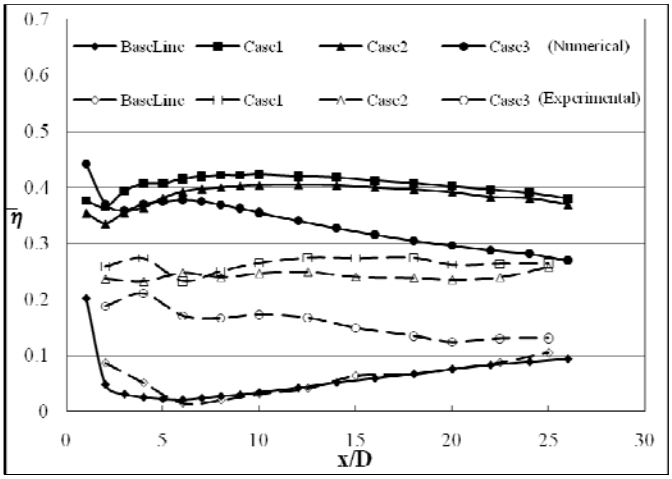

Figure (11) Effect of Anti Vortex Hole Geometry on Spanwise Averaged Film Cooling Effectiveness Distributions at VR = 2.0

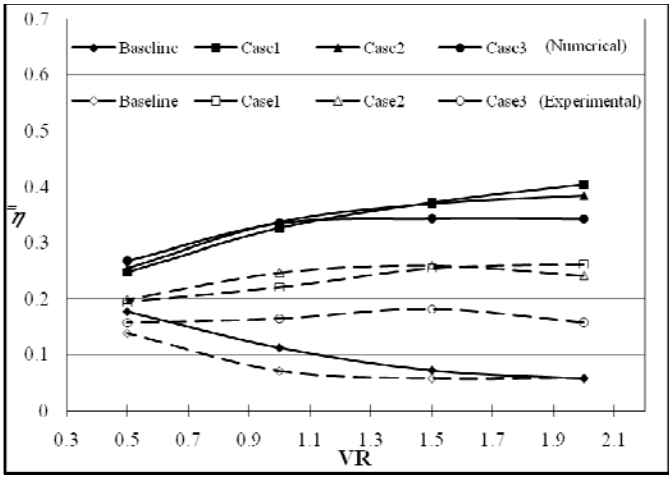

Figure (12) The overall averaged area film cooling effectiveness for all studied cases with different velocity ratios

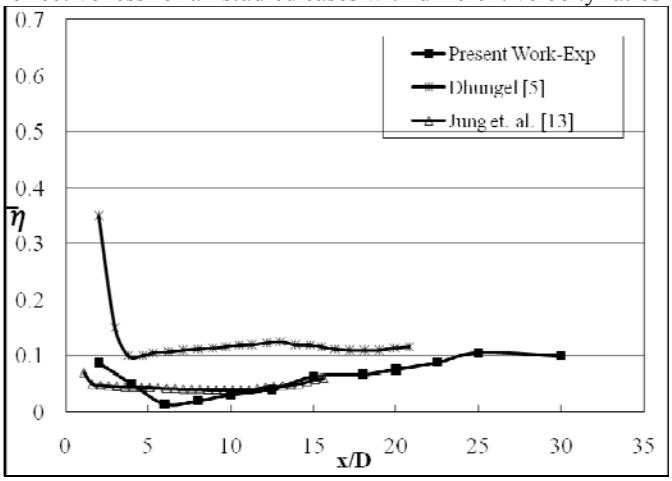

Figure (13) Comparison of Spanwise averaged film cooling effectiveness distribution for baseline, VR = 2.0

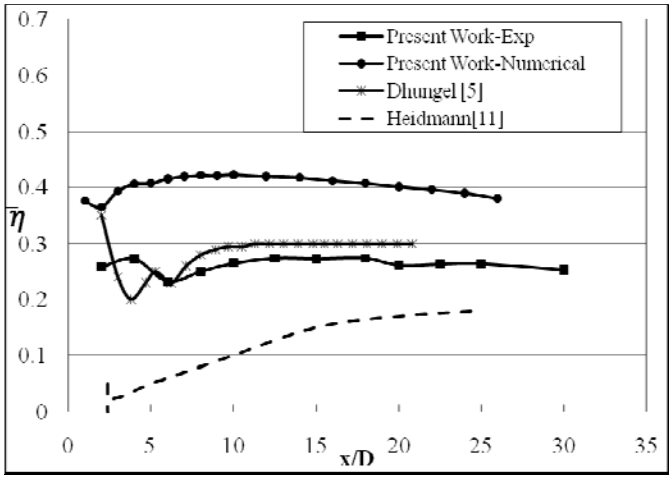

Figure (14) Comparison of Spanwise averaged film cooling effectiveness distribution for case1, VR = 2.0

According to the above results, the use of anti-vortex holes gives more enhancement in film cooling effectiveness than that is given by the traditional film cooling holes. That means the use of anti-vortex holes will give more cooling for the turbine blades. Figure (15) helps to know how the anti-vortex holes work. The figure shows a comparison between the boundary layer velocity distributions colored by effectiveness for all cases at VR = 2.0. From numerical solution, the boundary layer velocity distribution is presented at x/D = 4 due to clear details of the interaction between the mainstream flow and the coolant jets. For Baseline, Figure (15) shows two vortices due to the interaction between the mainstream flow and the coolant jet. As the velocity ratio increases, the two vortices lift off the coolant jet away from the test surface due to high momentum flux.

For Case 1, Figure (15) shows that there are new vortices, from the anti-vortex holes, appears above the two vortices coming out from the main hole. The new vortices try to move against the main hole vortices keeping the coolant flow near the test surface. This action is very clear with high velocity ratios. Case 2 has the same velocity vectors like case 1 because the anti-vortex holes are still upstream the main hole. But, it is clearly that the flow from the anti-vortex holes is moving beside the flow from the main hole and creates new vortices against the main hole vortices covering a wider area than that of case 1.

For case 3, the fluid flow from the anti-vortex holes is moving below the fluid flow from the main hole because the anti-vortex holes are in line with the main hole and have a less momentum flux than the main hole. So, the two vortices coming out from the main hole are lifting off by the flow from the anti-vortex holes.

Figure (16) gives more understanding for the above discussion. It shows the film cooling effectiveness distribution at test surface and x/D = 2, 8, and 15 for VR = 2.

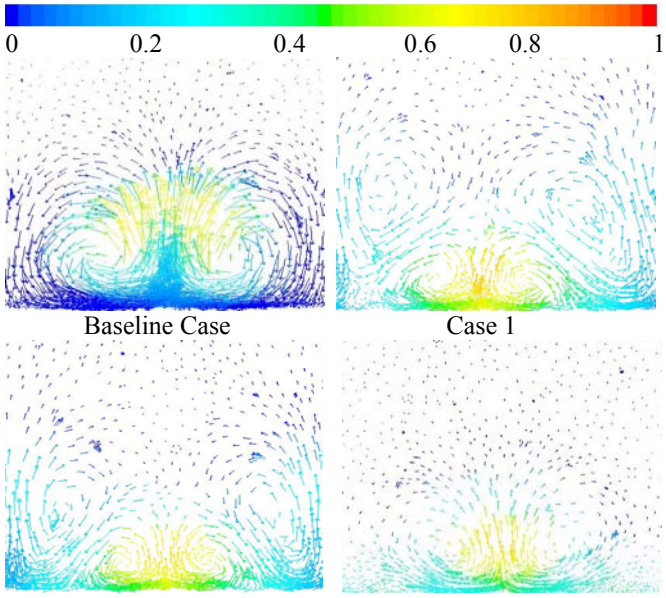

Figure (15) Secondary flow vectors colored by Effectiveness for studied cases VR = 2.0, x/D = 4

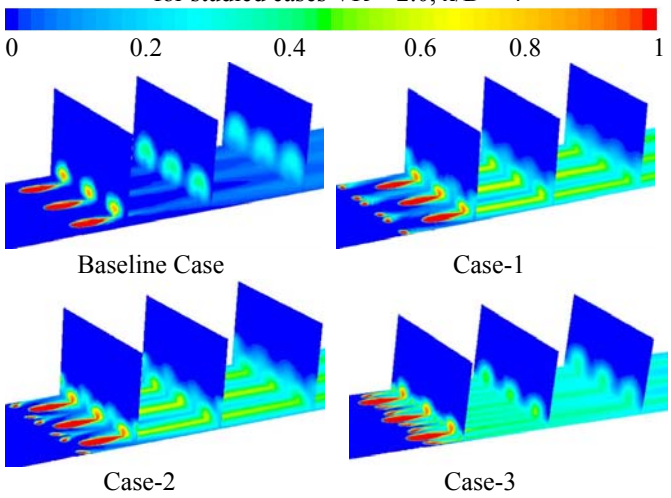

Figure (16) the detailed the film cooling effectiveness distribution at test surface and x/D = 2, 8, and 15 for VR = 2

CONCLUSIONS

A low speed wind tunnel is constructed to study experimentally the effect of using anti-vortex holes branching out from the main film cooling holes on the film cooling effectiveness. Also a computational code is used to study the same effect numerically. The following points represent the final conclusions.

1. The Results show that the use of anti-vortex holes enhance the film cooling downstream the film cooling holes. It appears that the presence of anti vortex holes mitigates the effect of the kidney vortices and also reduces the momentum of the main jet hence improving the film coverage in both downstream and lateral direction.
2. For baseline case, as the velocity ratio increases, the overall averaged area film cooling effectiveness decreases. But when the anti-vortex technique is applied, the overall averaged area film cooling effectiveness increases as the velocity ratio increases.
3. When the anti-vortex holes are upstream the main film cooling hole like in (Case 1 and 2), the film cooling covers more area as compared with case 3 in which the anti-vortex holes are in line with the main film cooling hole, especially, with high velocity ratios.
4. There is a good agreement between experimental and numerical results with about 2.3% deviation at VR = 2.0 and 21.7% at VR = 0.5 for baseline case. And about 34.9% at VR = 2.0 and 21.6% at VR = 0.5 for case 1.
5. The behavior of the interaction between the coolant jet and the mainstream flow is interpreted from the numerical solution.

As an extension to the present work, it is recommended to:

1. Study the effect of anti-vortex holes on curved turbine surface in a linear blade cascade.
2. The effect of wake passing effect may be added to the study due to its effect on the flow turbulence.

Also the effect of turbine blade rotation should be taken in consideration in the future works.

NOMENCLATURE

BR	Blowing Ratio =($\rho_c U_c/\rho_m U_m$)
D	Film cooling main hole diameter
d	Film cooling anti-vortex hole diameter
MR	Momentum Ratio = ($\rho_c U_c^2/\rho_m U_m^2$)
Re_D	Injectant Reynolds number = Uc*D/ν_c
Re_x	Free stream Reynolds number = U_m*x/ν_m
T_{aw}	Adiabatic wall temperature
T_c	Coolant air temperature
T_f	Local film temperature
T_m	Mainstream air temperature
U_c	Coolant air velocity
U_m	Mainstream air velocity
VR	Velocity Ratio = U_c/U_m
x	Distance from the film hole centerline

Greek Symbols

η	Film cooling effectiveness
$\bar{\eta}$	Average film cooling effectiveness
$\bar{\bar{\eta}}$	Overall film cooling effectiveness
ν	Kinematic viscosity of the fluid

Abbreviations

Ex	Experimental
Nu	Numerical

REFERENCES

[1] Ammari, H. D., Hay, N., and Lampard, D., "The Effect of Density Ratio on the Heat Transfer Coefficient from a Film Cooled Flat Plate." ASME Journal of Turbomachinery, Vol. 112, pp444-450, 1990.

[2] Andreopoulous, J. and Rodi, W., "Experimental Investigation of Jets in Crossflow Journal of Fluid Mechanics", Vol 138, pp 93-127, 1984.

[3] Bons, J.P., MacArthur, C.D., and Rivir, R.B., "The Effect of High Free-Stream Turbulence on Film Cooling Effectiveness." ASME Journal of Turbomachinery, Vol.118, pp.814-825, 1996.

[4] Bunker, R. S., "A Review of Shaped Hole Turbine Film-Cooling Technology," ASME J. Heat Transfer, 127, pp. 441–453, 2005.

[5] Dhungel, A., "Film Cooling from a Row of Holes Supplemented with Anti Vortex Holes" A Thesis for the degree of Master of Science in Mechanical Engineering, Louisiana State University, 2007.

[6] Dhungel, S., Phillips, A., Ekkad, S. V., and Heidmann, J. D., "Experimental Investigation of a Novel Anti-Vortex Film Cooling Hole Design," ASME Paper No. GT2007–27419, 2007.

[7] FLUENT 6.2.16 Guide Book, 2005

[8] Foster, N.W., Lampard, D., "The Flow and Film Cooling Effectiveness Following Injection Through a Row of Holes", ASME Journal of Eng. Power 102, pp. 584-588, 1980.

[9] Goldstein, R. J., Eckert, E. R. G., Eriksen, V. L., and Ramsey, J. W., "Film Cooling Following Injection Through Inclined Circular Tubes," Israel Journal of Technology, Vol. 8, No. 1–2, pp. 145–154, 1970.

[10] Haven, B. A., Yamagata, D. K., Kurosaka, M., Yamawaki, S., and Maya, T., "Anti-Kidney Pair of Vortices in Shaped Holes and Their Influence on Film Cooling Effectiveness," ASME Paper No. 97-GT-45, 1997.

[11] Heidmann, J. D., "A Numerical Study of Anti-Vortex Film Cooling Designs at High Blowing Ratio" NASA/TM—2008-215209, 2008.

[12] Heidmann, J. D., Ekkad, S., "A Novel Antivortex Turbine Film-Cooling Hole Concept" Journal of Turbomachinery, ASME, JULY 2008, Vol. 130, 2008.

[13] Jung, I. S., and Lee J. S., "Effects of Orientation Angles on Film Cooling Over a Flat Plate: Boundary Layer Temperature Distributions and Adiabatic Film Cooling Effectiveness" Journal of Turbomachinery, ASME, Vol.122, pp 153 – 160, 2000.

[14] Kline, S.J. and McClintock, F.A., "Describing Uncertainties in Single Sample Experiments," Mechanical Engineering, Vol. 75, pp. 3-8, 1953.

[15] Kohli, A., Bogard, D., "Adiabatic Effectiveness Thermal fields and Velocity Fields for Film Cooling with Large Angle Injection", ASME Journal of Turbomachinery, 119 pp.352-358, 1997.

[16] Lemmon, C. A., Kohli, A., and Thole, K. A., "Formation of Counter-Rotating Vortices in Film-Cooling Flows" ASME Paper No. 99-GT-161, 1999.

[17] Leylek, J.H., and Zerkle, R.D., "Discrete-jet Film Cooling: A Comparison of Computational Results with Experiments." ASME Journal of Turbomachinery, Vol. 116, pp358-368, 1994.

[18] Mehendale, A.B., and Han, J.C., "Influence of High Mainstream Turbulence on Leading Edge Film Cooling Heat Transfer: Effect of Film Hole Spacing," Int. J. of Heat Mass Transfer, 35, No. 10, pp. 2593-2604, 1992.

[19] Ou, S., Han, J.C., Mehendale, A.B., and Lee, C.P., "Unsteady Wake Over a Linear Turbine Blade Cascade with Air and CO2 Film Injection. Part I: Effect on Heat Transfer Coefficients." ASME J. Turbomachinery, 116, pp. 721-729, 1994.

[20] Yiping Lu, "Effect of Hole Configurations on Film Cooling from Cylindrical Inclined Holes for The Application to Gas Turbine Blades", partial fulfillment of the requirements for the degree of Doctor of Philosophy, Louisiana State University, 2007.